Atmos. Chem. Phys. Discuss., 10, 26607–26640, 2010
www.atmos-chem-phys-discuss.net/10/26607/2010/
doi:10.5194/acpd-10-26607-2010

Atmospheric Chemistry and Physics Discussions

Iron dissolution kinetics of mineral dust at low pH during simulated atmospheric processing

Z. Shi[1], S. Bonneville[1], M. D. Krom[1], K. S. Carslaw[2], T. D. Jickells[3], A. R. Baker[3], and L. G. Benning[1]

[1]Earth and Biosphere Institute, School of Earth and Environment, University of Leeds, Leeds, UK
[2]Institute of Climate and Atmospheric Sciences, School of Earth and Environment, University of Leeds, Leeds, UK
[3]School of Environmental Sciences, University of East Anglia, Norwich, UK

Received: 18 October 2010 – Accepted: 22 October 2010 – Published: 8 November 2010

Correspondence to: Z. Shi (shizongbo@163.com)

Published by Copernicus Publications on behalf of the European Geosciences Union.

Abstract

We investigated the iron (Fe) dissolution kinetics of African (Tibesti) and Asian (Beijing) dust samples at acidic pH with the aim of reproducing the low pH conditions in atmospheric aerosols. The Beijing dust and three size fractions of the Tibesti dust (<20 µm: PM_{20}; <10 µm: PM_{10}; and <2.5 µm: $PM_{2.5}$) were dissolved at pH 1, 2 and/or 3 for up to 1000 h. In the first 10 min, all dust samples underwent an extremely fast Fe solubilisation. Subsequently, the Fe dissolution proceeded at a much slower rate before reaching a stable dissolution plateau. The time-dependant Fe dissolution datasets were best described by a model comprising three acid-extractable Fe pools each dissolving according to first-order kinetics. The dissolution rate constant k of each pool was independent of the source (Saharan or Asian) and the size (PM_{20}, PM_{10} or $PM_{2.5}$) of the dust but highly dependent on pH. The "fast" Fe pool had a k ($25\,h^{-1}$ at pH=1) of a similar magnitude to "dry" ferrihydrite nanoparticles and/or poorly crystalline Fe(III) oxyhydroxide, while the "intermediate" and "slow" Fe pools had k values respectively 50–60 times and 3000–4000 times smaller than the "fast" pool. The "slow" Fe pool was likely to consist of both crystalline Fe oxide phases (i.e., goethite and/or hematite) and Fe contained in the clay minerals. The initial mass of the "fast", "intermediate" and "slow" Fe pools represented respectively about 0.5–2%, 1–3% and 15–40% of the total Fe in the dust samples. Furthermore, we showed that in systems with low dust/liquid ratios, Fe can be dissolved from all three phases, whereas at high dust/liquid ratios (e.g., in aerosols), sufficient Fe is solubilised from the "fast" phase to dominate the Fe dissolved and to suppress the dissolution of Fe from the other Fe pools. These data demonstrated that dust/liquid ratio and pH are fundamental parameters controlling Fe dissolution kinetics in the dust. In order to reduce errors in atmospheric and climate models, these fundamental controlling factors need to be included.

ACPD

10, 26607–26640, 2010

1 Introduction

Iron is an important limiting micronutrient for phytoplankton growth in the ocean (Martin et al., 1994; Boyd et al., 2007, 2010). Even though the Fe in dust represents only a small fraction of total Fe inputs to oceans, it is disproportionately important in open ocean waters (Jickells et al., 2005). In remote parts of the oceans, dust and their associated bio-available Fe pools can regulate key biogeochemical interactions and thus the feedbacks between the ocean and atmosphere, which in turn influences the climate (Martin et al., 1994; Jickells et al., 2005; Boyd et al., 2007; Moore et al., 2009). While the importance of atmospheric dust in the Fe supply to the oceans is now recognized, the actual quantification of the flux of dissolved Fe from mineral dusts remains one of the major uncertainties of the global Fe connections in the Earth System (Jickells et al., 2005; Mahowald et al., 2005; Boyd et al., 2010).

Measurements of the partial solubility of Fe (defined as the dissolved to total Fe fraction in%) in aerosols collected over oceans showed that this varies dramatically from ~0.1 to 80% (Hand et al., 2004; Baker and Jickells, 2006). These variations suggest that atmospheric processes during long-range transport strongly affect and increase aerosol dust Fe solubility (Mahowald et al., 2005). One of the potential processes leading to this increase is the acidification of the aqueous matter associated with aerosols (e.g., Zhu et al., 1992; Meskhidze et al., 2003). In the atmosphere, mineral aerosols can take up sulfate and/or nitrate (Sullivan et al., 2007; Shi et al., 2008). These particles then become effective cloud condensation nuclei and thus may be processed in clouds, where in turn more acid can be taken up (Manktelow et al., 2010). Furthermore, when the cloud droplets evaporate, most of the water is lost, leading to an increase in the relative concentration of the dissolved acids and therefore a drop in pH, with values as low as pH 1 or lower having been suggested in fine dust aerosols or measured in fine marine aeosols (e.g., Zhu et al., 1992; Keene et al., 2002). Furthermore, it has been shown that even some stratocumulus clouds can be acidic, i.e., having a pH of ~3 (e.g., Hegg et al., 2002; Straub et al., 2007).

ACPD
10, 26607–26640, 2010

Fe-rich dust particles are often smaller in size than the median size particles in a dust event (Cwiertny et al., 2008; Ogata et al., 2010), which means that they can be transported for longer distance and have more time and surface area to take up acids. In addition, since Fe-rich dust particles are often externally mixed (physically separated) with calcite and dolomite (Sullivan et al., 2007), acids that are taken up by bulk dust aerosols would not be automatically neutralized by carbonate. Therefore, Fe-rich dust particles are more likely to experience low pH conditions during their long-range transport (Ito and Feng, 2010). Several recent atmospheric aerosol measurements of Fe and Al solubilities supported the importance of acid-promoted dissolution of mineral dust (Measures et al., 2010; Hsu et al., 2010).

Models of the role of acid processing on the enhancement of Fe solubility in dust after long range transport have suggested that the acidic nature of the material associated with the dust particles can, to some extent, explain the observed higher partial Fe solubility in dust collected above the open ocean compared to that observed close to the dust source area (Hand et al., 2004; Solmon et al., 2009; Ito and Feng, 2010). However, most modelling studies (Luo et al., 2005; Fan et al., 2006; Solmon et al., 2009; Ito and Feng, 2010) have assumed a simplistic and monomineralic dust Fe mineralogy (e.g., all Fe in dust is assumed to be present as pure hematite) and they also assumed a zero-order dissolution kinetics for this hematite. We have clearly shown that assuming that all Fe in dust samples is present as a single mineral phase is incorrect and that such assumptions can lead to large errors (~500%) in predicting the Fe solubility in real samples (Shi et al., 2010).

The dissolution kinetics and equilibrium solubilities of a large range of pure Fe(III) oxides and oxyhydroxide mineral phases have been measured experimentally (Cornell and Schwertmann, 2003; Bonneville et al. 2009). However, these datasets cannot be directly applied to global dust models because dust samples are usually composed of a variable mixture of Fe minerals that have a variety of sizes as well as mineralogical and chemical compositions (Shi et al., 2010). Furthermore, the experimental conditions used for the above-mentioned Fe dissolution studies are most often not relevant to the

ACPD
10, 26607–26640, 2010

processes in the atmosphere. In particular, dust which is normally transported in the atmosphere for days to a couple of weeks (Mahowald et al., 2005; Uno et al., 2009; Solmon et al., 2009) is unlikely to reach true thermodynamic equilibrium (Cornell and Schwertmann, 2003). It is thus important to develop an understanding of the kinetics of Fe dissolution in real dust samples. Such studies need to be carried out under experimental conditions relevant to and as representative as possible of atmospheric processes.

The purpose of this study was to determine the Fe dissolution kinetics in mineral dusts under acidic conditions, which simulate as closely as possible the atmospheric processes. We measured the Fe dissolution kinetics in different dust samples from the Sahara and Asia at different pH and dust/liquid ratios. Various kinetic models were tested to fit the pH- and time-dependant Fe dissolution data and based on this we proposed a new way to describe the Fe dissolution in mineral dusts. Finally, we discussed the Fe dissolution behaviour of Fe containing mineral phases in our dust samples in view of their applicability to describing and modelling atmospheric processes.

2 Materials and methodology

2.1 Dust samples

A soil sample (hereafter termed Tibesti) was collected from a dry river bed (N25°35' E16°31') draining the Tibesti Mountains (South Libya) and periodically subjected to flash flood. The area where the sample was collected has been shown to be a major source of dust by both TOMS and Meteosat IDDI (Prospero et al., 2002; Schepanski et al., 2007). The sample was dry-sieved to <63 µm and then wet-sieved to <20 µm (Tibesti-PM_{20}) with MilliQ water. The wet sample suspension was freeze dried and later gently disaggregated before use. We used the Tibesti-PM_{20} as a surrogate for mineral dust. Lafon et al. (2006) has shown that the geochemical properties of PM_{20} were similar to those of the PM_{10} (<10 µm) from size fractionation experiments

ACPD
10, 26607–26640, 2010

obtained in a wind tunnel. Using a custom-made particle re-suspension system, we also separated the original soil samples into Tibesti-PM_{10} and Tibesti-$PM_{2.5}$ (<2.5 µm), respectively. The details of the particle re-suspension system were given in Jones et al. (2010).

An Asian dry-deposited dust sample (hereafter termed Beijing dust) was collected after a super-dust storm episode on 17 April 2006 from a pre-cleaned surface on the campus of China University of Mining and Technology (Beijing), Beijing, China (N 39°60′, E 116°21′).

2.2 X-ray Fluorescence (XRF) analysis

Major elements were determined by XRF. Results are quoted as component oxide weight percent (Table 2). Samples were analysed at the University of Leicester, Department of Geology on a PANalytical Axios Advanced XRF spectrometer calibrated using international and internal standards. A lake sediment standard (LKSD-1) yielded a total elemental recovery of 98% with accuracy for all elements of better than 10%, except for P_2O_5 which was 16% compared to quoted reference values (Shi et al., 2010). We used the total Fe content termed hereafter FeT (after re-calcutating the XRF provided wt% Fe_2O_3 to mol% Fe) for all relevant calculations in this study.

2.3 Sequential Fe extraction

In order to fully characterise the speciation of Fe in the dust samples, a standard geochemical leaching procedure was used (Hyacinthe et al., 2006; Raiswell et al., 2008). The first step in this procedure is to extract the chemically highly reactive/labile Fe phases, which are usually amorphous and/or poorly crystalline. This was done by reacting 15 mg of a sample for 24 hours with 10 mL of ascorbate solution buffered to pH 7.5. The extractant solution was a deoxygenated solution of 50 g L^{-1} sodium citrate and 50 g L^{-1} sodium bicarbonate to which 10 g L^{-1} of ascorbic acid was added. This highly labile Fe fraction is hereafter referred to as FeA. After reaction with this ascorbate

ACPD
10, 26607–26640, 2010

solution, the samples were filtered through 0.2 µm polycarbonate filters. The particles collected on the filters were subsequently extracted for 2 h with a solution of 50 g L^{-1} sodium dithionite in 0.35 M acetic acid and 0.2 M sodium citrate (CBD), buffered at pH 4.8. This extraction dissolves the crystalline Fe(III) oxides, mainly goethite and hematite. The Fe phases in this second fraction are less labile than the FeA fraction, but they are more reactive than the Fe containing silicate phases (Hyacinthe et al., 2006; Raiswell et al., 2008). The Fe pool obtained by this second extraction is hereafter referred to as FeD. The sum of these two pools (FeA+FeD) is defined as the reducible Fe. The precision of both extraction methods was tested using nine Arizona Test Dust replicates (Power Tech. Ltd., USA) which gave 0.067±0.005% (7.5% r.s.d 1s $n = 9$) for FeA and 0.41±0.04% (9.7% r.s.d., 1s, $n = 9$) for FeD (Shi et al., 2009, 2010).

After each reaction step, the dissolved Fe concentrations (FeA and FeD) in the filtered solutions were determined via the ferrozine method (Volier et al., 2000). Dissolved Fe measurements of replicate samples gave a precision of ±1.2% (1s $n = 6$).

2.4 Fe dissolution experiments

In order to determine the Fe dissolution kinetics in our samples, three sets of time dependent dissolution experiments were performed. These were (i) the dissolution of Tibesti-PM_{20} and Beijing dust samples at pH 1, 2 and/or 3 for up to 1000 h, (ii) the dissolution of Tibesti samples of different size fractions at pH 1 for up to 800 hours, and (iii) the dissolution of a Beijing dust sample at various dust/liquid ratios at pH 1 for up to 24 hours. For the first set of experiment (i), 60 mg of dust (Beijing or Tibesti-PM_{20}) were added to 1 L of 0.1, 0.01, and 0.001 N H_2SO_4 solutions made from Titrosol solutions (hereafter designated as pH 1, 2, and 3; Note: the pH of a 0.1 N H_2SO_4 solution is slightly higher than 1 due to the effect of ionic strength on the activity of H^+). In the grain size effect experiments (ii), we reacted each of the three different sizes of the Tibesti dust (PM_{20}, PM_{10} and $PM_{2.5}$) with a pH 1 solution at a dust/liquid ratio of 60 mg L^{-1}. In our last experimental set (iii), we explored the effect of varying dust/liquid ratios on the Fe dissolution kinetics in our experimental system, by reacting

ACPD
10, 26607–26640, 2010

10 and 1000 mg L^{-1} of Beijing dust with a pH 1 solution (in addition to the experiment at 60 mg L^{-1} – in set i). In all experiments the pH remained stable within the measurement capability of the used pH meter (i.e., 0.1 pH unit).

For comparison, we also quantified the dissolution kinetics of (a) a synthesized fresh ferrihydrite at pH 1 and 2, and (b) a standard illite sample which was pre-cleaned by reacting with the CBD method described in Sect. 2.3 to remove any Fe oxides potentially present in the sample (Shi et al., 2010) at pH 2. The fresh ferrihydrite was used as a reference Fe(III) oxyhydroxide and was synthesized following the method in Cornel and Schwertmann (2003), while the standard illite sample was obtained from clay mineral depository (http://www.clays.org/SOURCE%20CLAYS/SCavailable.html).

All experiments were performed at room temperature under constant stirring (~50 rpm) in dark conditions. In order to follow the Fe dissolution kinetics, aliquots of the suspensions were regularly collected and filtered through a 0.2 µm pore size membrane filter directly into 2 N HCl (final concentration of ~0.2 N HCl) in order to preserve the dissolved Fe for subsequent ferrozine analyses (Voillier et al. 2000). To confirm that the filtration procedure efficiently removed all suspended nanoparticles from solution, during an experiment at pH 1, three aliquots from a 60 mg L^{-1} Tibesti-PM_{20} suspension were filtered after 3 min, 10 min, and 1 h, and half of each filtrate solution was acidified to ~0.2 N HCl. The Fe concentrations were measured immediately after filtration (within 10 min, non-acidified) but also after 2 weeks storage in 0.2 N HCl. No systematic increase in Fe concentrations was observed indicating that the filtration was effective.

3 Results and discussion

3.1 Sample characteristics

Table 1 lists the chemical composition and Fe speciation of the Beijing and Tibesti-PM_{20} samples. Compared to Tibesti-PM_{20}, the Beijing dust contained more SiO_2 (~58

ACPD
10, 26607–26640, 2010

vs. 49%) and less Al_2O_3 (12 vs. 18%). In the Tibesti-PM_{20} sample the FeA fraction (amorphous and poorly crystalline Fe) accounted for only 0.6%, while in the Beijing dust sample FeA reached 1.7%. The crystalline Fe oxides (FeD) were 22.3 and 37.7% of the total Fe in the Beijing dust and the Tibesti-PM_{20} sample, respectively.

The reducible Fe to total Fe ((FeA+FeD)/FeT) in the Tibesti-PM_{20} sample (0.38, Table 1) was close to the average ratio measured for atmospheric dust samples originated from the Sahara (0.35±0.07; Lazaro et al., 2008). Therefore, although originally the Tibesti sample was sourced from a soil, the Tibersti-PM_{20} fraction can be considered representative of dust from the Sahara (Shi et al., 2010). The Beijing dust sample is a typical Asian dust sample since its mineralogical composition is similar to samples collected during other major dust storms in Beijing (Shi et al., 2005; Shao et al., 2008).

3.2 Fe dissolution kinetics

Figure 1 shows the Fe dissolution kinetics of Tibesti-$PM_{2.5}$, Tibesti-PM_{10}, and Tibesti-PM_{20} at pH 1. In the three experiments, the initial period of dissolution was extremely fast (see inset in Fig. 1) with the dissolved Fe concentrations reaching ~17 and ~32 µmol g^{-1} of dust after 0.5 h for Tibesti-PM_{20} and $PM_{2.5}$, respectively. Subsequently, the dissolved Fe concentrations increased at a slower rate before reaching a plateau after ~400 h at ~275 µmol g^{-1} for Tibesti-PM_{10} and PM_{20} and ~350 µmol g^{-1} for $PM_{2.5}$.

For Beijing dust and Tibesti-PM_{20} the Fe dissolution rate was strongly pH-dependant. At pH 1 and pH 2, after a sharp increase during the first 3 h, the dissolved Fe concentrations increased gradually towards a plateau (Fig. 2), while at pH 3 the Fe dissolution proceeded at a slower rate from the beginning of the experiment. At pH 1 after 450 h, the dissolved Fe levelled off at ~275 µmol g^{-1} while at pH 2 and 3 both Beijing dust and Tibesti-PM_{20} were still dissolving after 800 and 1000 h, respectively. At pH 2, the Beijing dust sample exhibited a slightly higher solubility than Tibesti-PM_{20} (i.e. at 800 h~175 vs 125 µmol g^{-1}).

ACPD
10, 26607–26640, 2010

The effect of the dust/solution ratio (10, 60 and 1000 mg L^{-1}) on Fe dissolution in the Beijing dust sample at pH 1 is illustrated in Fig. 3. For the three dust/liquid ratios, the dissolution proceeded as described above with a fast initial phase followed by a slower continuous increase in the dissolved Fe concentrations. In addition, although the dissolved Fe concentration was in all cases normalized per mass of dust, we observed that, as the dust/liquid ratio increased, the observed concentration in solution was lower suggetsing that the dissolution had slowed down. For example, after 20 h the dissolved Fe concentration reached around 80 µmol g^{-1} for 10 mg L^{-1} compared to half that (40 µmol g^{-1}) for 1000 mg L^{-1}.

3.3 Kinetic models of dust Fe dissolution

Many models have been developed to describe the dissolution kinetics of Fe minerals under different conditions (Cornel and Schwertmann, 2003). Among them, the reactive continuum model, developed initially to describe the degradation of organic matter in sediments (Boudreau and Ruddick, 1991), has been used extensively to describe the time-dependant release of Fe from sediment and oxides during chemical extractions (Boudreau and Ruddick, 1991; Postma et al, 1993; Larsen and Postma, 2001; Hyacinthe and Van Cappellen, 2004; Hyacinthe et al., 2006). Initially we applied this kinetic model to the Fe dissolution curves of the different samples (e.g., Fig. 4 for Tibesti-$PM_{2.5}$) and fitted the time-dependent release of Fe according to:

$$\frac{J}{M(0)} = \frac{v}{a}\left(\frac{M(0)-M(t)}{M(0)}\right)^{1+\frac{1}{v}} \quad (1)$$

where J, v/a, and $1+1/v$ are the dissolution rate (µmol g^{-1} s^{-1}), apparent rate constant (s^{-1}), and apparent reaction order, respectively. $M(0)$ (in µmol g^{-1}) stands for the initial concentration of extractable Fe present in the dust sample, and $M(t)$ (in µmol g^{-1}) is the corresponding concentration in solution at time t. This rate law is derived under the assumption that the initial reactivity distribution of the mineral assemblage follows a gamma function (see Appendix A in Hyacinthe and Van Capellen (2004) for details

ACPD
10, 26607–26640, 2010

of the derivation of Eq. (1) from the gamma distribution proposed in Boudreau and Ruddick (1991)). The resulting time evolution of $M(t)$ is then given by:

$$M(t) = M(0) - M(0)\left(\frac{a}{a+t}\right)^{v} \quad (2)$$

Optimized values of the parameters v, a and $M(0)$ were determined by fitting the time-dependent dissolution data to Eq. (2), following the method in Hyacinthe and Van Cappellen (2004) but with $M(t)$ representing the Fe in solution.

Although at first, such a reactive continuum model seemed to describe reasonably well the measured data (r^2>0.95), a closer examination of the Fe concentration profile at the beginning of the reactions (first 12 h, insert figure in Fig. 4) showed that the continuum model drastically underestimated the dissolved Fe concentrations in this part of the reaction. Conversely, between 50 and 400 h, the reactive continuum model overestimated the actual Fe concentrations. As the initial part of the Fe dissolution (<12 h) is important in term of atmospheric aerosol processes, the use of the reactive continuum model in this context is problematic.

Hyacinthe et al. (2006) suggested that this type of fitting problem using the reactive continuum model is due to the presence of two or more Fe pools of different dissolution reactivities (more than one order of magnitude difference). The reactive continuum model is unable to describe adequately such a multiphase system (Hyacinthe et al., 2006). In dust, the existence of several different Fe pools is very likely as Fe may be dissolved from poorly crystalline and more crystalline Fe oxides as well as clay minerals which are known to exhibit distinct reactivities in term of Fe dissolution (e.g. Journet et al, 2008). To solve this fitting problem and to accurately describe the Fe dissolution curves in our experiments, we applied the formalism proposed by Hyacinthe et al. (2006) and used a combination of Fe pools each dissolving according to different first-order kinetic rates. We fitted our Fe dissolution curves with a cumulative dissolution approach with initially two and then three pools of Fe according to:

$$M_t = \sum (M_0 - M_0 \times e^{-kt}) \quad (3)$$

ACPD
10, 26607–26640, 2010

where M_t is the cumulative dissolved Fe concentration (unit: μmol g^{-1}) at time t, M_0 is the initial amount of a particular Fe pool in μmol g^{-1} of dust, and k is the dissolution rate constant, and t is the time. At each particular time, the total concentration of Fe solubilized represents the sum of the Fe dissolved from all the Fe pools. The use of two Fe pools improved the quality of the fit to the experimental Fe dissolution curves, but still significantly under-predicted the initial Fe dissolution profiles. The best results were obtained with a model assuming the simultaneous first-order dissolution of 3 Fe pools –"fast", "intermediate" and "slow" – with k values of 25, 0.5, and 0.005 h^{-1} and M_0 of 25, 30, and 290 μmol g^{-1} for the Tibesti-$PM_{2.5}$ sample (Fig. 5). This approach showed a good fit even during the initial time period (inset, Fig. 5). The Root Mean Square of the error (RMS) – an indicator of the fit quality – decreased from 30.7 for the reactive continuum model to 11.2 using the 2-Fe pool model and finally 5.0 with the 3-Fe pool model. Using the 3-Fe pool model, we then fitted the Fe dissolution curves of all the other samples and for the different pH conditions (Table 2 lists the k and M_0 values used). As an element of comparison, the Fe dissolution curves of the two standard materials (i.e., fresh ferrihydrite and illite) were fitted with a first-order dissolution model but as they were pure end member minerals only a single Fe pool approach was required.

Our results demonstrated that, under acidic conditions, the Fe dissolution kinetics of samples from two of the major sources of dust in the world (Asia and Sahara) can be accurately described using a simple cumulative model assuming first-order dissolution kinetics of 3 acid-extractable pools of Fe. To further explore the consequences of this we will address (1) how and why the modelling parameters, k and M_0, change as a function of pH, dust/liquid ratio and size, (2) what the potential mineralogical compositions of the proposed 3 Fe pools may be, and (3) how well the current Fe dissolution parameterizations used in atmospheric models perform against the kinetic data presented above.

ACPD
10, 26607–26640, 2010

3.4 Kinetic parameters for modelling dust dissolution kinetics at low pH

Our 3-Fe pools model provided a range of rate constant values (k) and the amount of each acid-extractable pool (M_0) which accurately characterize the Fe dissolution kinetics of the two dust samples, for a range of pH values (1, 2 and/or 3) and sizes (PM_{20}, PM_{10}, and $PM_{2.5}$) (Table 2).

The k provides a quantification of the reactivity of the three kinetically defined Fe pools. Our results show that k values for each Fe pool are independent of the source of the sample (i.e. Asian or African dust) or of grain size. For instance, the k is $25\,h^{-1}$ for the "fast" pool at pH 1 for both the Beijing and Tibesti-PM_{20} but also in Tibesti-PM_{10} and Tibesti-$PM_{2.5}$. The observation is also valid for the "intermediate" and the "slow" pools of acid-extractable Fe. It seems therefore that our kinetic description based on three Fe pools is able to capture the Fe dissolution behavoir in natural dusts accurately.

Not surprisingly, the derived k values are strongly pH-dependant (Fig. 6) and the different pools can be expressed as pH dependent equations:

$$\log k_{\text{"fast" Fe pool}} = -0.50\,\text{pH} + 1.87 \quad (4)$$

$$\log k_{\text{"intermediate" Fe pool}} = -0.66\,\text{pH} + 0.36 \quad (5)$$

$$\log k_{\text{"slow" Fe pool}} = -0.44\,\text{pH} - 1.76. \quad (6)$$

The M_0 values in Table 2 represent the quantity of Fe of a specific pool that can be dissolved at a particular dissolution condition (e.g., pH) and M_0 was also pH-dependent and generally decreased with increasing pH in a same sample (Table 2). For the "fast", "intermediate" and "slow" Fe pools, M_0 at pH 1 and 2 represent respectively about 0.9–2.9%, 2.1–3.5% and 18.5–43.2% of the total Fe in the Beijing dust and the Tibesti-PM_{20} samples.

To better understand how the amount of Fe solubilised (M_0) varies with pH, we plotted the sum of M_0^* (note that M_0^* (in $\mu\text{mol}\,L^{-1}$) is re-calculated from M_0), representing here the equilibrium Fe concentration for experiments carried out at $60\,\text{mg}\,L^{-1}$ for the

ACPD
10, 26607–26640, 2010

Beijing dust sample, with the equilibrium Fe solubilities of a series of Fe oxides over a range of pH values (Fig. 7). We were surprised to find that the sum of M_0^* , representing the equilibrium Fe concentration of the real dust sample at a given pH (i) only decreased by a factor 2–3 between pH 1 to 3 (compared to nearly 3 orders of magnitude change per pH unit for major Fe oxides) and (ii) was much lower (several orders of magnitude) compared to equilibrium Fe solubilities of major Fe oxides (Fig. 7). These results indicate that the plateau observed in Fig. 2 (equivalent to the sum of M_0^* values) does not represent the equilibrium Fe solubility in a thermodynamic sense. The reason is that there were not enough reactive Fe minerals in the dust samples when dissolved at low dust/liquid ratios (i.e., 60 mg L^{-1}) to reach thermodynamic equilibrium. For example, if all the "fast" Fe pool, which was 1.2% of FeT in the Tibesti-PM_{20} sample (Table 2), was dissolved, this pool only represented a concentration of 0.6 µmol L^{-1} Fe in solution at a dust/liquid ratio of 60 mg L^{-1}. This is 6 orders of magnitude smaller than the equilibrium Fe solubility of ferrihydrite at pH 1 (see Fig. 7). In fact, at pH 1, even if all the Fe in the dust (i.e., FeT) at a dust/solution ratio of 60 mg L^{-1} would be solubilised – which equates to 51 µmol L^{-1}, the Fe concentration would still not have reached equilibrium Fe solubilities of most Fe oxides (see right horizontal lines in Fig. 7).

The above discussion points to the critical role of the dust/solution ratio in influencing the extent and the kinetics of Fe dissolution from dust at low pHs. It is important to distinguish the dissolved Fe concentration in µmol L^{-1} from the proportion of Fe solubilised in µmol g^{-1} of dust. In terms of dissolved Fe concentration (in µmol L^{-1}), the Fe dissolution kinetics of a 1000 mg L^{-1} dust suspension is much faster than 60 mg L^{-1} and a fortiori 10 mg L^{-1} due to a much larger reactive surface area present in the system. However, when considering the fraction of Fe solubilised (i.e. µmol Fe g^{-1} of dust) as illustrated in Fig. 3, increasing dust/solution ratios from 10 to 1000 mg L^{-1} lead to a decrease in the amount of Fe dissolved per mass of dust especially at exposure times over 1 h. Under dilute conditions and low pH (e.g., <20 mg L^{-1}), the proportion of Fe dissolved per mass of dust is independent of the dust/liquid ratio (Machie et al., 2005), and therefore the dissolved Fe concentration (in µmol L^{-1}) is linearly dependent

ACPD
10, 26607–26640, 2010

on the mass of dust in the solution. This is because the dissolved Fe concentration (in μmol L^{-1}) in the solution is strongly under-saturated with respect to the equilibrium solubilities of most Fe oxides so that the Fe dissolution is not thermodynamically restricted (Fig. 7). By contrast, at very high dust/liquid ratios (e.g., 300 g L^{-1}), which may occur in wet dust aerosols, dissolved Fe concentrations (in μmol L^{-1}) derived solely from the "fast pool" would already be extremely high even at pH 2. In the case of the Beijing dust, this would reach 1740 μmol L^{-1} (assuming a M_0 of 5.8 μmol g^{-1}, Table 2) surpassing largely the equilibrium Fe solubilities of nanogoethite and hematite at pH 2 (Fig. 7). Thus, under those conditions (also valid for higher pH), the two latter phases would stop to dissolve. Thus we conclude that the effect of dust/liquid ratio on the dissolution behaviour of Fe in dusts follows a complex pathway in that: (i) in dilute systems, the dissolved Fe is the sum of the Fe solublised from the three phases present, (ii) however at high dust/liquid ratios, sufficient Fe is dissolved from the "fast" phase to suppress the dissolution of Fe from the "intermediate" and "slow" Fe pools.

The size of dust is another potentially important factor affecting Fe dissolution kinetics. Baker and Jickells (2006) suggested that gravitational settling of coarse dust particles across the Atlantic away from the Saharan source lead to an increase in operationally defined Fe solubility (Fe dissolved after a 1.5–2 h ammonium acetate leach at pH 4.7). They hypothesized that their observation was due to a larger surface to volume ratio of the finer dust particles. In the current study we observed that within dust particles, the proportion of "fast" and "intermediate" Fe pools (highly reactive Fe pools) increased: from 10.5 and 18 μmol g^{-1} for PM_{20}, to 18 and 25 μmol g^{-1} for PM_{10}, to 25 and 30 μmol g^{-1} in $PM_{2.5}$ from the Tibesti sample (Table 2). This dependence is likely to be the result of mineralogical fractionation: with "fast" and "intermediate" Fe pools which we interpret as being nanoparticles (<100 nm; see below) (Cornell and Schwertmann, 2003; Shi et al., 2010) which are slightly enriched in the Tibesti-$PM_{2.5}$ compared to the Tibesti-PM_{20}. Therefore, our results suggest that the gravitational settling of large, Fe-depleted, particles tends to produce a small increase in dissolved Fe per mass of dust from PM_{20} to $PM_{2.5}$. However, a full investigation of partial Fe

ACPD
10, 26607–26640, 2010

solubility in the dust over a full range of grain sizes is needed to fully address this " gravitational settling " hypothesis proposed by Baker and Jickells (2006).

3.5 Link between Fe mineralogy and the three Fe pools

One of the important questions in dust Fe dynamic is to identify the source(s) of the dissolved Fe. In a strict sense, the three Fe pools identified in this study are defined only according to their Fe dissolution kinetics. In order to identify the mineralogy of the different Fe pools, we examined whether their dissolution kinetics were similar to known Fe phases found in soil/dust.

Freshly prepared ferrihydrite, a highly reactive Fe(III) oxides, was dissolved under equivalent experimental conditions as our dust samples and the measured rate constant k decreased from 120 to 27 h^{-1} at pH 1 and 2, respectively. These k values were about 4-5 times larger than those of the "fast" Fe pool of our dust samples at the corresponding pH (Fig. 6). Therefore, the "fast" Fe pool is unlikely to be solely made up of "fresh" ferrihydrite. However, ferrihydrite upon drying and storage has been shown to lose its reactivity (by a factor of up to 3 orders of magnitude) and dry ferrihydrite is much less reactive to dissolution than fresh ferrihydrite (Raiswell et al., 2010). Since fresh ferrihydrite, if any, in our dust samples was unlikely to be present (samples were taken from the Sahara desert during normal dry and hot conditions prior to storage for months to a couple of years in the lab before our dissolution experiments), we hypothesize that the "fast" Fe pool in our dust samples was likely primarily composed of somewhat less reactive dry ferrihydrite and/or poorly crystalline Fe(III) oxyhydroxides. This behaviour is supported by the fact than the M_0 of the "fast" Fe pool for Beijing and Tibesti – PM_{20} (~0.9 and 1.2% of FeT) were relatively close to the amount of Fe solubilized with pH-buffered ascorbate extraction (FeA) yielding ~1.7 and ~0.6% of the FeT. It is known that ascorbate selectively extracts amorphous and/or poorly crystalline Fe oxides (Hyacinthe et al., 2006; Raiswell et al., 2008), and this has been confirmed from the analyses of a series of soil/dust across the Sahara desert (Shi et al., 2009, 2010).

ACPD
10, 26607–26640, 2010

The rate constant k of an illite standard was comparable to that of the "slow" Fe pool: 0.0036 versus 0.0022 at pH 2 (Table 2 and Fig. 7). This suggests that illite and potentially other clay minerals may be an important component of the "slow" Fe pool. On the other hand, at pH 1 and 60 mg L^{-1}, Fe dissolved from the Beijing dust sample did not reach the value predicted for hematite equilibrium Fe solubility (Fig. 7). Thus, these results indicate that the "slow" Fe pool represents both crystalline Fe oxide phases (goethite and/or hematite) and Fe-containing clay minerals.

Based on our data it is difficult to assign a particular type of mineral for the "intermediate" Fe pool. However, this Fe pool exhibited a reactivity between that of the "fast" and "slow" pools. We speculate here that the "intermediate" pool was mainly composed of nano-sized Fe oxides, which have been found in natural soil dust samples (Shi et al., 2010) and which are known to have a reactivity between highly crystalline/larger size Fe oxides and poorly crystalline Fe oxides (Rubasinghege et al., 2010; Schwertmann, 1991).

Overall, our results confirm our previous work (Shi et al., 2010) showing that partial Fe solubility based on short-term acidic Fe dissolution cannot be predicted adequately from a simple consideration of the bulk mineralogy of a particular sample as suggested by Journet et al. (2008). Here we have shown that the initial Fe dissolution is actually driven predominantly by "fast" and "intermediate" Fe pools. This poses a real challenge to studies of Fe biogeochemistry in dust since they represent only a small fraction of FeT and are probably present as nanometer particles dispersed in the dust.

3.6 Implications and outlook

Several modelling studies have simulated the importance of acidic processing of mineral dust in transforming insoluble Fe into labile Fe (Meskhidze et al., 2005; Luo et al., 2005; Fan et al., 2006; Solmon et al., 2009; Ito and Feng, 2010). These authors assumed that Fe existed only as hematite and applied one or a series of zero-order dissolution rates measured on crystalline hematite. Our results demonstrate that the Fe dissolution in two representative dust samples (Saharan and Asian) did not follow

ACPD
10, 26607–26640, 2010

a zero-order reaction. We found that the Fe initial dissolution was extremely fast (at a dust/liquid ratio <1g L^{-1}), and this can not be described adequately with a zero-order dissolution kinetic model (Fig. 8). The simplistic approach may lead to a significant under-estimation in the beginning of the Fe dissolution and potentially over-estimation at later stages. In particular the slow zero-order dissolution rate for the first 0-0.8% of the total Fe in the dust used in these atmospheric models (Meskhidze et al., 2005; Luo et al., 2005; Solmon et al., 2009; Ito and Feng, 2010), was in contrast to our data as well as others (Spokes et al., 1994; Desboeufs et al., 2005; Machie et al., 2005; Cwiertny et al., 2008; Fu et al. 2010). It also needs to be mentioned that effect of dust/liquid ratio on the Fe dissolution was not considered in the present models.

If M_0 and k for each Fe pool is known, then one can calculate the amount of Fe solubilized from the mineral dust at low pH conditions. As discussed above, k at low pHs can be calculated using Eqs. (2)–(4). However, the values for M_0 for each of the pools is dependent on many factors: the pH, the dust/liquid ratio, and the size of the dust. The pH and the particle size of dust could potentially be predicted using a global model (e.g., Solmon et al., 2009; Manktelow et al., 2010). However, the dust/liquid ratios are extremely variable as dust cycles between clouds with a low ratio and aerosols with higher ratios. For example, the dust/solution ratio in the rainwater was calculated to vary from 75 µg L^{-1} to 9.6 g L^{-1} (e.g., Baker et al., 2007; Ozsoy et al., 2009), while in wet aerosols, dust/solution ratio are expected to be higher, e.g., >300 g L^{-1}. To calculate the amount of dissolved Fe deposited to the oceans, it is also necessary for a model to estimate the exposure time at different pH conditions as well as the dust/solution ratio during the dust lifetime. Being able to predict these parameters remains a big challenge, although some global aerosol microphysics models do already simulate at least the size-resolved mixing state of dust particles (Manktelow et al., 2010) and could be extended to simulate also the solution pH and dissolution kinetics.

In addition, the source and nature of the dust may also affect Fe dissolution (Shi et al., 2010). In the present study we have measured the dissolution kinetics of two

ACPD
10, 26607–26640, 2010

representative dust samples, which have rather similar rates of Fe dissolution (Fig. 2) in line with the moderate degree of weathering (as measured through the Parker index, Table 1). However dust samples from highly weathered areas, like the Sahel region, may have very different dissolution kinetics. Indeed, Fe dissolution behaviour of Australian dusts appeared to be different compared to ours (Machie et al., 2005), which is potentially due to discrepancies in Fe mineralogy. Finally, although pH appears to be one of the most important factors at the same dust/liquid ratio, photo-reduction and complexation of Fe by organic compounds and the type of acids in the aerosol may also affect Fe dissolution in dust (Siefert et al., 1994; Spokes et al., 1996; Machie et al., 2005; Rubasinghege et al., 2010; Fu et al., 2010).

In summary, we have established in this study that (1) there is an extremely reactive Fe pool in both African and Asian dust samples, which dissolves at low pH conditions very quickly; (2) Fe dissolution kinetics in the dust at low pH conditions is dependent on dust/liquid ratio, pH , and to a less extent the size of the dust particles; (3) in order to reduce errors, models need to consider the complexity of Fe dissolution in the dust.

Acknowledgements. This work was supported by NERC (NE/E011470/1, PI: Krom). S. Bonneville and L. G. Benning achnowledge the financial support from NERC (NE/C004566/1; PI: Benning). R. Mortimer, S. Shaw, and R. Raiswell at University of Leeds are acknowledged for their comments or technical help. We thank T. Jones and H. Chuang from Cardiff University for providing access to a particle resuspension system. L. Shao and W. Li at China University of Mining and Technology are thanked for collecting the Beijing dust sample. Thanks are paid to N. Meskhidze at North Carolina State University for useful discussions related to this work.

References

Baker, A. R., Weston, K., Kelly, S. D., Voss, M., Streu, P., and Cape J. N.: Dry and wet deposition of nutrients from the tropical Atlantic atmosphere: Links to primary productivity and nitrogen fixation, Deep-Sea Res. I, 54, 1704-1720, 2007.

Baker, A. R. and Jickells, T. D.: Mineral particle size as a control on aerosol iron solubility, Geophys. Res. Lett., 33, L17608, doi:10.1029/2006GL026557, 2006.

ACPD

10, 26607–26640, 2010

Bonneville, S, Behrends, T., Van Cappellen, P.: Solubility and dissimilatory reduction kinetics of iron(III) oxyhydroxides: A linear free energy relationship, Geochim. Cosmochim. Ac., 73, 5273–5282, 2009.
Boudreau, B. P. and Ruddick, B. R.: On a reactive continuum representation of organic matter diagenesis, Am. J. Sci., 291, 507–538, 1991.
Boyd, P., Jickells, T. D., Law, C. S., Blain, S., et al.: Mesoscale iron enrichment experiments 1993-2005: synthesis and future directions, Science, 315, 612–617, 2007.
Boyd, P. W. and Ellwood, M. J.: The biogeochemical cycle of iron in the ocean, Nature Geosci., 3, 675-682, doi:10.1038/ngeo964, 2010.
Cornell, R. M., Posner, A. M., and Quirk, J. P.: Kinetics and mechanisms of the acid dissolution of goethite (α-FeOOH), J. Inorg. Nucl. Chem., 38, 563–567, 1976.
Cornell, R. M. and Schwertmann, U.: The Iron Oxides: Structure, Properties, Reactions, Occurrence and Uses, Wiley-VCH Publishers, New York, USA, 201–220; 345–364; 297–344, 2003.
Cwiertny, D. M., Baltrusaitis, J., Hunter, G. J., Laskin, A. Scherer, M. M., Grassian, V. H.: Characterization and acid-mobilization study of iron-containing mineral dust source materials, J. Geophys. Res., 113, D05202, 2008.
Desboeufs, K. V., Sofikitis, A., Losno, R. Colin, J. L., and Ausset, P.: Dissolution and solubility of trace metals from natural and anthropogenic aerosol particulate matter, Chemosphere, 58, 195–203, 2005.
Fan, S.-M., Moxim, W. J., Levy II, H.: Aeolian input of bioavailable iron to the ocean, Geophys. Res. Lett., 33, L07602, 2006.
Fu. H., Cwiertny, D. M., Carmichael, G. R., Scherer, M. M., and Grassian, V. H.: Photoreductive dissolution of Fe-containing mineral dust particles in acidic media, J. Geophy. Res., 115, D11304, doi:10.1029/2009JD012702, 2010.
Hand, J. L., Mahowald, N. M., Chen, Y., Siefert, R. L., Luo, C., Subramaniam, A., and Fung, I.: Estimates of atmospheric-processed soluble iron from observations and a global mineral aerosol model: Biogeochemical implications, J. Geophys. Res., 109, D17205, doi:10.1029/2004JD004574, 2004.
Hegg, D. A., Gao, S., and Jonsson, H.: Measurements of selected dicarboxylic acids in marine cloud water, Atmos. Res., 62, 1–10, 2002.
Hsu, S. C., Wong, G. T. F., Gong, G. C., Shiah, F. K., Huang, Y. T., Kao, S. J., Tsai, F., Lung, S. C. C., Lin, F. J., and Lin, I. I.: Sources, solubility, and dry deposition of aerosol trace elements

ACPD
10, 26607–26640, 2010

over the East China Sea, Marine Chem., 120, 116–127, 2010.
Hyacinthe, C., Bonneville, S., and Van Cappellen, P.: Reactive Iron (III) in sediments: Chemical versus microbial extractions, Geochim. Cosmochim. Ac., 70, 4166–4180, 2006.
Hyacinthe, C. and Van Cappellen, P.: An authigenic iron phosphate phase in estuarine sediments: composition, formation and chemical reactivity, Mar. Chem., 91, 227–251, 2004.
Ito, A. and Feng, Y.: Role of dust alkalinity in acid mobilization of iron, Atmos. Chem. Phys., 10, 9237–9250, doi:10.5194/acp-10-9237-2010, 2010.
Jickells, T. D., An, Z. S., Andersen, K. K., Baker, A. R., Bergametti, G., Brooks, N., Cao, J. J., Boyd, P. W., Duce, R. A., Hunter, K. A., Kawahata, H., Kubilay, N., LaRoche, J., Liss, P. S., Mahowald, N., Prospero, J. M., Ridgwell, A. J., Tegen, I., Torres, R.: Global iron connections between desert dust, ocean biogeochemistry, and climate, Science, 308, 67–71, 2005.
Jones, T., Brown, P., BeruBe, K., Wlodarczyk, A., and Shao, L.: The physicochemistry and toxicology of CFA particles, J. Toxicol. Environ. Health A, 73(5), 341–354, 2010.
Journet, E., Desboeufs, K. V., Caquineau, S., and Colin, J.-L.: Mineralogy as a critical factor of dust iron solubility, Geophys. Res. Lett., 35, L07805, doi:10.1029/2007GL031589, 2008.
Lafon, S., Sokolik, I. N., Rajot, J. L., Caquineau, S., and Gaudichet, A.: Characterization of iron oxides in mineral dust aerosols: Implications for light absorption, J. Geophys. Res., 111, D21207, doi:10.1029/2005JD007016, 2006.
Larsen, O. and Postma, D.: Kinetics of reductive bulk dissolution of lepidocrocite, ferrihydrite, and goethite, Geochim. Cosmochim. Acta, 65, 1367–1379, 2001.
Luo, C., Mahowald, N. M., Meskhidze, N., Chen, Y., Siefert, R. L., Baker, A. R., and Johansen, A. M.: Estimation of iron solubility from observations and a global aerosol model, J. Geophys. Res., 110, D23307, doi:10.1029/2005JD006059, 2005.
Mackie, D. S., Boyd, P. W., Hunter, K. A., and McTainsh, G. H.: Simulating the cloud processing of iron in Australian dust: pH and dust concentration, Geophys. Res. Lett., 32, L06809, doi:10.1029/2004GL022122, 2005.
Mahowald, N. M., Baker, A. R., Bergametti. G., Brooks, N., Duce, R. A., Jickells, T. D., Kubilay, N., Prospero. J. M., and Tegen, I.: Atmospheric global dust cycle and iron inputs to the ocean, Global Biogeochem. Cy., 19, GB4025, doi:10.1029/2004GB002402, 2005.
Manktelow, P. T., Carslaw, K. S., Mann, G. W., and Spracklen, D. V.: The impact of dust on sulfate aerosol, CN and CCN during an East Asian dust storm, Atmos. Chem. Phys., 10, 365–382, doi:10.5194/acp-10-365-2010, 2010.
Martin, J. H., Coale, K. H., Johnson, K. S., et al.: Testing the iron hypothesis in ecosystems of

ACPD
10, 26607–26640, 2010

the equatorial Pacific Ocean, Nature, 371, 123–129, 1994
Meskhidze, N., Chameides, W. L., and Nenes, A.: Dust and pollution: A recipe for enhanced ocean fertilization?, J. Geophys. Res., 110, D03301, doi:10.1029/2004JD005082, 2005.
Meskhidze, N., Chameides, W. L., Nenes, A., and Chen, G.: Iron mobilization in mineral dust: Can anthropogenic SO2 emissions affect ocean productivity?, Geophys. Res. Lett., 30, 2085, doi:10.1029/2003GL018035, 2003.
Moore, C. M., Mills M. M., Achterberg, E. P., Geider, R. J., LaRoche, J., Lucas, M. I., McDonagh, E. L., Pan, X., Poulton, A. J., Rijkenberg, M. J. A., Suggett, D. J., Ussher, S. J., and Woodward, E. M. S.: Large-scale distribution of Atlantic nitrogen fixation controlled by iron availability, Nat. Geosci., 2, 867–871, 2009.
Keene, W. C., Pszenny, A. A. P., Maben, J. R., and Sander, R.: Variation of marine aerosol acidity with particle size, Geophy. Res. Lett., 29(7), 1101, doi:10.1029/2001GL013881, 2002.
Ogata, H., Zhang, D., Yamada, M., and Tobo, Y.: Comparison of elemental composition of Asian dust particles at Amami and Amakusa during a dust event, J. Jpn. Soc. Atmos. Environ., accepted, 2010.
Ozsoy, T. and Ornektekin, S.: Trace elements in urban and suburban rainfall, Mersin, Northeastern Mediterranean, Atmos. Res., 94, 203–219, 2009.
Postma, D.: The reactivity of iron oxides in sediments: a kinetic approach, Geochim. Cosmochim. Ac. 57, 5027–5034, 1993.
Prospero, J. M., Ginoux, P., Torres, O., Nicholson, S. E., and Gill, T. E.: Environmental characterization of global sources of atmospheric soil dust dandified identified with the NIMBUS 7 Total Ozone Mapping Spectrometer (TOMS) absorbing aerosol product, Rev. Geophys., 40(1), 1002, doi:10.1029/2000RG000095, 2002.
Raiswell, R., Vu, H. P., Brinza, L., and Benning, L. G.: The determination of labile Fe in ferrihydrite by ascorbic acid extraction: methodology, dissolution kinetics and loss of solubility with age and de-watering, Chem. Geo., 278, 20–79, doi:10.1016/j.chemgeo.2010.09.002, 2010.
Raiswell, R., Benning, L. G., Tranter, M., and Tulaczyk, S.: Bioavailable iron in the Southern Ocean: the significance of the iceberg conveyor belt, Geochem. Trans., 9(7), doi:10.1029/2000RG000095, doi:10.1.1186/1467-4866-9-7, 2008.
Rubasinghege, G., Lentz, R. W., Scherer, M. M., and Grassian, V. H.: Simulated atmospheric processing of iron oxyhydroxide minerals at low pH: Roles of particle size and acid anion in iron dissolution, PNAS, 107, 6628–6633, 2010.
Schepanski, K., Tegen, I., Laurent, B., Heinold, B., and Macke, A. L.: A new Saharan dust

ACPD
10, 26607–26640, 2010

source activation frequency map derived from MSG-SEVIRI IR channels, Geophys. Res. Lett., 34, L18803, doi:10.1186/1467-4866-9-7, 2007.
Schwertmann, U.: Solubility and dissolution of iron oxides, Plant Soil, 130, 1–25, 1991.
Shao, L., Li, W., Xiao, Z., and Sun, Z.: The mineralogy and possible sources of spring dust particles over Beijing, Adv. Atmos. Sci., 25, 395–403, 2008.
Shi, Z., Shao, L., Jones, T. P., and Lu, S.: Microscopy and mineralogy of airborne particles collected during severe dust storm episodes in Beijing, China, J. Geophys. Res., 110, D01303, doi:10.1029/2004JD005073, 2005.
Shi, Z., Zhang, D., Hayashi, M., Ogata, H., Ji, H., and Fujiie, W.: Influences of sulfate and nitrate on the hygroscopic behaviour of coarse dust particles, Atmos. Environ., 42, 822–827, doi:10.1016/j.atmosenv.2007.10.037, 2008.
Shi, Z., Krom, M. D., Bonneville. S., Baker, A. R., Jickells, T. D., and Benning, L. G.: Formation of iron nanoparticles and increase in iron reactivity in the mineral dust during simulated cloud processing, Environ. Sci. Technol., 43, 6592–6596, doi:10.1021/es901294g, 2009.
Shi, Z., Krom, M. D., Bonneville, S., Baker, A. R., Bristow, C., Drake, N., Mann, G., Carslaw, K., McQuaid, J. B., Jickells, T., Benning, L. G.: Influence of chemical weathering and aging of iron oxides on the potential iron solubility of Saharan dust during simulated atmospheric processing, Global Biogeochem. Cy., under review, 2010.
Siefert, R. L., Pehkonen, S. O., Erel, Y., Hoffmann, M. R.: Iron photochemistry of aqueous suspensions of ambient aerosol with added organic acids, Geochim. Cosmochim. Ac., 58, 3271–3279, 1994.
Solmon, F., Chuang, P. Y. Meskhidze, N., Chen, Y.: Acidic processing of mineral dust iron by anthropogenic compounds over the north Pacific Ocean, J. Geophys. Res., 114, D02305, doi:10.1029/2008JD010417, 2005.
Spokes, J. L., Jickells, T. D., Lim, B.: Solubilisation of aerosol trace metals by cloud processing: A laboratory study, Geochim. Cosmochim. Ac., 58, 3281–3287, 1994.
Spokes, L. J. and Jickells, T. D.: Factors controlling the solubility of aerosol trace metals in the atmosphere and on mixing into seawater, Aqua. Geochem., 1, 355–374, 1996.
Straub, D. J., Lee, T., and Collett Jr., J. L.: Chemical composition of marine stratocumulus clouds over the eastern Pacific Ocean, J. Geophys. Res., 112, D04307, doi:10.1029/2006JD007439, 2007.
Stumm, W. and Furrer, G.: The dissolution of oxides and aluminium silicates: Examples of surface-coordination-controlled kinetics, in: Aquatic surface chemistry, Stumm, W., John Wi-

ACPD
10, 26607–26640, 2010

ley & Sons, New York, USA, 197–219, 1987.
Sullivan, R. C., Guazzotti, S. A., Sodeman, D. A., and Prather, K. A.: Direct observations of the atmospheric processing of Asian mineral dust, Atmos. Chem. Phys., 7, 1213–1236, doi:10.5194/acp-7-1213-2007, 2007.
Uno, I., Eguchi, K., Yumimoto, K., Takemura, T., Shimizu, A., Uematsu, M., Liu, Z., Wang, Z., Hara, Y., and Sugimoto, N.: Asian dust transported one full circuit around the globe, Nature Geosci., 2, 557–560, 2009.
Viollier, E., Inglett, P. W., Hunter, K., Roychoudhury, A. N., and Van Cappellen, P.: The ferrozine method revisited: Fe(II)/Fe(III) determination in natural waters, Appl. Geochem., 15, 785–790, 2000.
Wieland, E. and Stumm, W.: Dissolution kinetics of kaolinite in acidic aqueous solutions at 25°C, Geochim. Cosmochim. Ac., 56, 3339–3355, 1992.
Zhu, X., Prospero, J. M., Millero, F. J. Savoie, D. L., and Brass, G. W.: The solubility of ferric ion in marine mineral aerosol solutions at ambient relative humidities, Mar. Chem., 38, 91–107, 1992.

ACPD
10, 26607–26640, 2010

Table 1. Chemical composition of major elements, FeA, FeD, reducible Fe, and Parker weathering index of Beijing and Tibesti-PM_{20} sample.

	SiO_2	TiO_2	Al_2O_3	Fe_2O_3	MnO	MgO	CaO	Na_2O	K_2O	P_2O_5	SO_3	LOI	Total	FeA	FeD	Reducible Fe ratio	Parker index
Beijing dust	57.8	0.7	12.3	5.0	0.1	2.5	6.0	1.9	2.3	0.2	0.1	11.2	100.0	1.71	22.3	24.0	211
Tibesti-PM_{20}	48.7	0.9	17.7	6.9	0.1	3.7	5.9	0.7	2.2	0.2	0.3	11.7	99.0	0.63	37.7	38.3	155

Notes: Units of oxides are in weight percentage. The FeA, FeD and reducible Fe (FeA+FeD) are given in percent of the total Fe content as determined by XRF. LOI means loss on ignition. Details about the calculation of the Parker index of chemical weathering are given in Shi et al. (2010).

ACPD
10, 26607–26640, 2010

Table 2. Rate constant k (h^{-1}) and initial amount of each Fe pool M_0 (in $\mu mol\,g^{-1}$) used to model the Fe dissolution curves of Beijing and Tibesti dust samples ($60\,mg\,L^{-1}$) and reference materials.

Sample and pH	Parameter	Fast	Intermediate	Slow	total
Tibesti-$PM_{2.5}$ (pH 1)	k	25	0.500	0.0062	
	M_0	25	30	290	345
	%FeT	2.9	3.5	33.9	40.4
Tibesti-PM_{10} (pH 1)	k	25	0.500	0.0062	
	M_0	18	25	235	278
	%FeT	2.1	2.9	27.5	32.5
Tibesti-PM_{20} (pH 1)	k	25	0.5	0.0062	
	M_0	10.5	18	245	273.5
	%FeT	1.2	2.1	28.7	32.0
Tibesti-PM_{20} (pH 2)	k	6.7	0.110	0.0022	
	M_0	10.5	18.0	130	158.5
	%FeT	1.2	2.1	15.2	18.5
Beijing dust (pH 1)	k	25.0	0.500	0.0062	
	M_0	5.8	19.0	270	294.8
	%FeT	0.9	3.0	43.2	47.2
Beijing dust (pH 2)	k	6.7	0.110	0.0022	
	M_0	5.8	19.0	175.0	199.8
	%FeT	0.9	3.0	28.0	32.0
Beijing dust (pH 3)	k	2.5	0.024	0.0008	
	M_0	3.2	6.2	80.0	89.4
	%FeT	0.5	1.0	12.8	14.3
Fresh ferrihydrite (pH 1)	k	120.0			
Fresh ferrihydrite (pH 2)	k	27.0			
Illite (pH 2)	k	0.0036			

Note:%FeT was calculated as the percentage of the mass of a particular Fe pool (in g) to total Fe (in g). The FeT of Tibesti-$PM_{2.5}$ and Tibesti-PM_{10} were not measured and Tibesti-PM_{20} FeT was used instead for calculating the percentage of Fe pool.

ACPD
10, 26607–26640, 2010

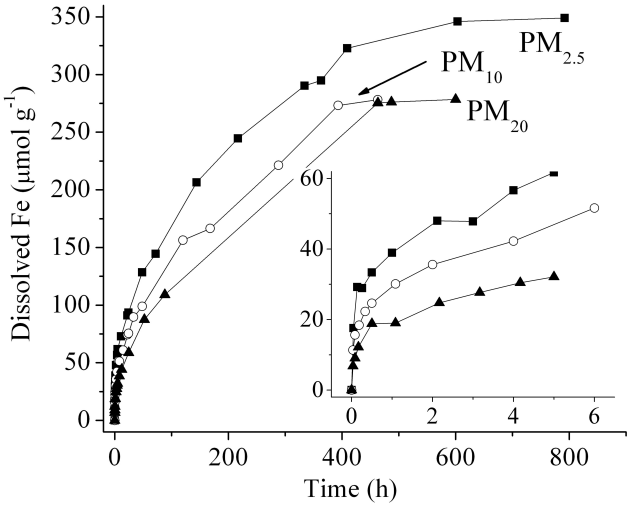

Fig. 1. Fe dissolution kinetics in Tibesti PM_{20}, PM_{10} and $PM_{2.5}$ at pH 1 and at a dust/liquid ratio of 60 mg L^{-1} . The inset shows the results from the first 6 h of the experiments in more detail.

ACPD
10, 26607–26640, 2010

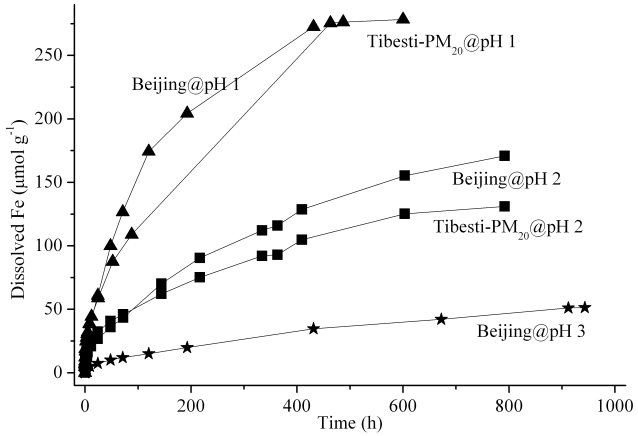

Fig. 2. Fe dissolution kinetics of Tibesti-PM_{20} and Beijing dust samples at pH 1, 2 and 3 and at a dust/liquid ratio of 60 mg L^{-1}.

ACPD
10, 26607–26640, 2010

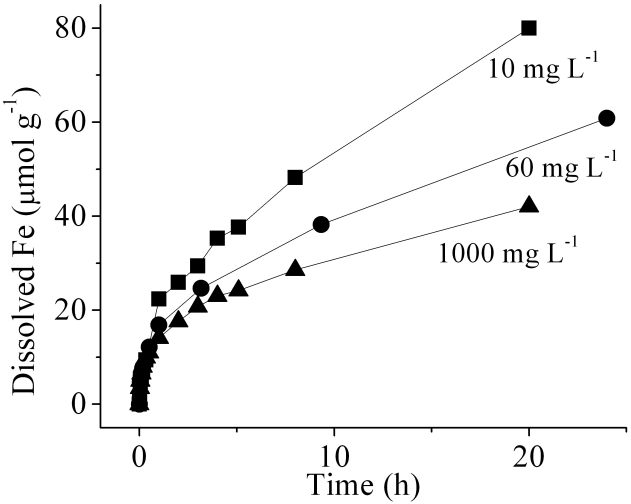

Fig. 3. Fe dissolution of Beijing dust at pH 1 at dust/solution ratios of 10, 60, and 1000 mg L^{-1}.

ACPD
10, 26607–26640, 2010

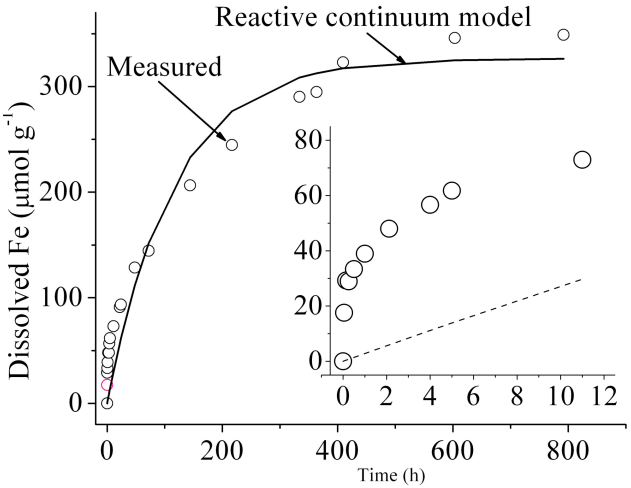

Fig. 4. Fitting of the Fe dissolution curve of Tibesti-$PM_{2.5}$ at pH 1 and a dust/liquid ratio of 60 mg L^{-1} using the reactive continuum model. The inset shows the measured Fe compared with the predicted values over the first 12 h of the experiments in more detail.

ACPD
10, 26607–26640, 2010

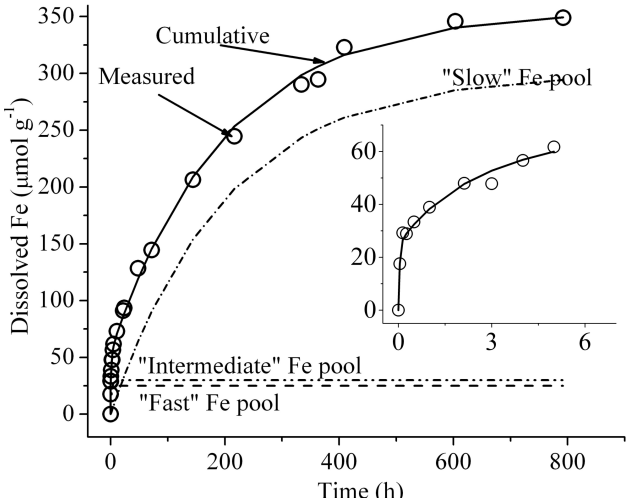

Fig. 5. Measured Fe dissolution curve with predicted curve of the Tibesti-$PM_{2.5}$ sample at pH 1 and at a dust/liquid ratio of 60 mg L^{-1} assuming a 3-Fe pool model. The inset shows the measured Fe compared with the calculated Fe from the 3-Fe pool over the first 6 h of the experiments in more detail.

ACPD
10, 26607–26640, 2010

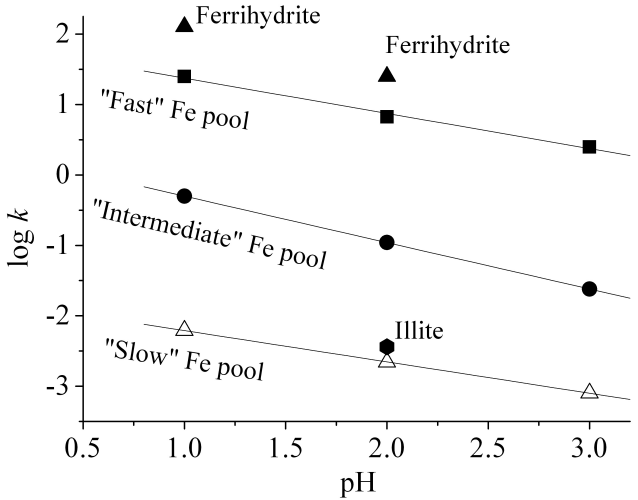

Fig. 6. Rate constant k for the three acid extractable pools as a function of pH. Solid lines represent linear regression for each of the three acid-extractable Fe pools.

ACPD
10, 26607–26640, 2010

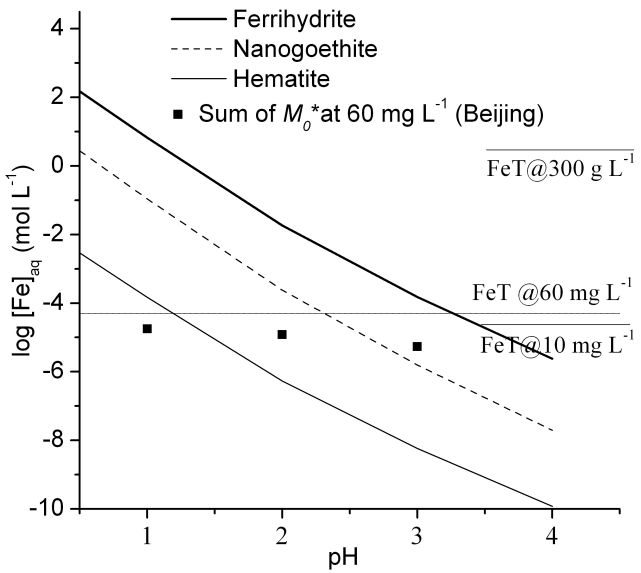

Fig. 7. Equilibrium Fe solubilities of a range of Fe(III) oxides between pH 0.5 and 4 versus the sum of M_0^* (i.e. "fast"+"intermediate"+"slow" Fe pools) at 60 mg L^{-1}. Solubilities for the hematite were from Bonneville et al. (2009). Fresh ferrihydrite and nanogoethite equilibrium Fe solubilities were experimentally measured at pH 3 and pH 2, respectively and further extrapolated to other pH values according to Bonneville et al. (2009). Horizontal solid lines represent the total Fe concentrations, if all of FeT in Beijing dust was solubilised for various dust/solution ratios (10 and 60 mg L^{-1}, and 300 g L^{-1}). Note that M_0^* in this figure has been recalculated from M_0 (Table 2) assuming an experimental concentration of 60 mg L^{-1}.

ACPD
10, 26607–26640, 2010

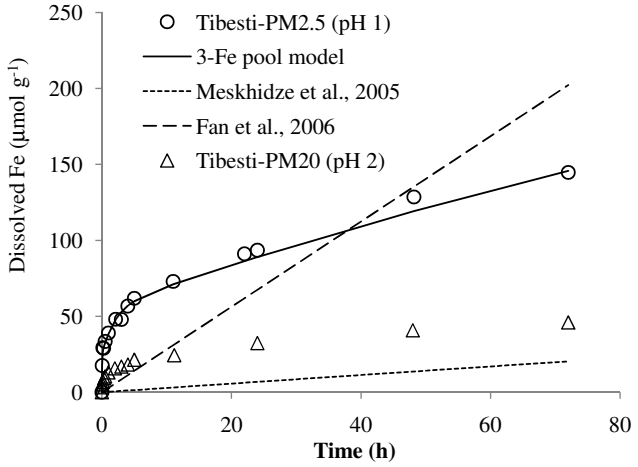

Fig. 8. Comparison of Fe dissolution curves predicted from rate constants used in Meskhidze et al. (2005) and Fan et al. (2006), and the actual measured ones for Tibesti-$PM_{2.5}$ at pH 1 and Tibesti-PM_{20} at pH 2. The curve to fit the measured data was from the 3-Fe pool model in this study. FeT content was assumed to be 4.8% and hematite surface area to be 100 $m^2\ g^{-1}$ for calculating Fe concentration using rate constants (in $mol\,m^{-2}\,s^{-1}$) in Meskhidze et al. (2005) and Fan et al. (2006).

ACPD
10, 26607–26640, 2010